L. Sartore, S. Pandini, F. Baldi, F. Bignotti, L. Di Landro
Biocomposites Based on Poly(lactic Acid) and Superabsorbent Sodium Polyacrylate
Journal of Applied Polymer Science, Vol. 134, N. 48, 2017, 045655 (9 pages)
doi:10.1002/app.45655

Biocomposites based on poly(lactic acid) and superabsorbent sodiumpolyacrylate

Luciana Sartore[1],Stefano Pandini[1],Francesco Baldi[1],Fabio Bignotti[1]

Luca Di Landro[2]

[1]Department of Mechanical and Industrial Engineering, University of Brescia Via Branze 38, Brescia 25133, Italy

[2]Department of Aerospace Science and Technology, Polytechnic of Milan, via La Masa 34, Milano 20156, Italy

ABSTRACT

In this research work, biocomposites based on crosslinked particles of sodium polyacrylate, commonly used as superabsorbent polymer, and poly(l-lactic acid) (PLLA) were developed to obtain superabsorbent thermoplastic products, and to elucidate the role of this type of filler (i.e., polymeric crosslinked particles) on their overall physical-mechanical behavior. Samples prepared by melt-blending components with different ratios showed a biphasic system with a uniform distribution of particles, with diameters up to about 50 μm, within the PLLA polymeric matrix. The polymeric biphasic system, coded PLASA, that is, superabsorbent PLLA, showed excellent swelling properties, demonstrating that crosslinked particles retain their superabsorbent ability even if distributed in a thermoplastic polymeric matrix. The thermal characteristics of the biocomposites evidenced enhanced thermal stability in comparison with neat PLLA and also mechanical properties are markedly modified by addition of crosslinked particles, revealing a regular stiffening effect. Furthermore, in aqueous environments the particles swell and are leached from PLLA matrix generating very high porosity. These new open-pore foams coded PLASAW, that is, PLASA after water treatment, produced in absence of organic solvents and chemical foaming agents, with good physicomechanical properties appear very promising for several applications, for instance in tissue engineering for scaffold production.

INTRODUCTION

Superabsorbent polymers (SAPs) are a class of special hydrogels, which exhibit the ability of swelling in water or aqueous solutions and retaining a significant fraction of water within their structure, without dissolving[1-3]. Crosslinked polymer gels have been widely developed as super absorbent materials since they may be successfully employed for application in many fields such as agriculture, hygienic products, waste-water treatment, drug-delivery, coal dewatering, and aircraft fuel treatment [4-11]. SAP is a three-dimensional crosslinked network formed by hydrophilic groups and organic groups of carbon chains which can absorb a large amount of water, allowing water uptakes up to several hundred times its initial value, and presenting excellent water retention even under some pressure[1].

So far, SAPs based on sodium acrylate and derivatives have been widely used for their convenient and inexpensive synthesis; the gel strength and elasticity are governed by the composition and the degree of crosslinking. However, conventional chemically crosslinked SAPs are usually brittle and weak, and this imposes some limits in their applications. Recent advances in strong and tough hydrogels as well as organic–inorganic nanocomposites [12-14] production allowed to overcome such a limitation and suggest the basis to promising systems for potential applications as SAP materials. However, most of those synthesis procedures are very complicated and expensive, and, thus, not suitable for being extensively used in common application. Despite the long history of SAPs in applications ranging from water purification, separation, and oil recovery, etc., the lack of strength and toughness of these materials has remained a challenge. After preparation, the gels are usually lyophilized and crushed into powders. However, SAP still encounters limitations for its poor processability due to its crosslinked structure. To overcome such limitations, in this article crosslinked SAP particles were used as a filler to prepare a composite thermoplastic material based on PLLA. To date in fact, PLA has gained enormous attention as a possible replacement for some conventional petroleum-based packaging materials [15]. PLA is derived from renewable resources, it is truly biodegradable and offers advantages thanks to a high clarity and displaying mechanical properties close to those of polystyrene and poly(ethylene terephthalate) [16]. Relevant applications of PLA as food packaging polymer for short shelf-life products are, for example, containers of fresh-cut products, lamination films, and blister packages [17]. In addition to packaging, there is a growing interest in using PLA for other industrial sectors such as fibers and automotive applications and especially for biomedical uses, in medicine and surgery [18,19]. The introduction of additional absorbent properties to PLA-based materials can further expand their range of applications, for example, as sanitary products, medical bandages, liquid absorbers in food packaging products, water blocking products in the construction industry.

In this article, PLA-based composites incorporating SAP particles were prepared by melt-blending with different amounts of superabsorbent particles. The effect of this superabsorbent filler incorporation was investigated on the composite morphology, on their thermal, mechanical, and rheological properties, as well as on their superabsorbent response. Furthermore, since particles tend to swell and be leached in water, the biocomposites may be considered as precursors for the safe (i.e., without organic solvents and chemical foaming agents) preparation of highly microporous PLLA, whose microstructure and mechanical properties were evaluated.

EXPERIMENTAL

Materials

Poly(l-lactic acid) (PLLA) was purchased from Nature Works (Blair, NE) and had a nominal weight-average molecular weight (M_w) of 199,590 Da and the brand name 2002D. The material was dried at 70 °C under vacuum for 12 h before use.
Crosslinked sodium polyacrylate was purchased from Evonik Industries AG (Essen, Germany) and had the brand name Produkt T 5066F; the particle size was lower than 63 μm and density is 0.7 g/cm^3. It was dried at 60 °C under vacuum for 12 h before use.

Sample Preparation

The dried PLLA and SAP particles were treated at 180 °C in a discontinuous mixer (Brabender, Plastograph, Duisberg, Germany) with a screw speed of 50 rpm, and the total mixing time was 6 min. The total polymer content inside the mixing chamber was 57 g, and four different weight percentages of SAP with respect to the total amount of PLLA were used to prepare SAP particles containing PLLA.
All samples were recovered from the mixing chamber and were kept in a vacuum at 50 °C for 24 h before being transformed in sheets by means of a laboratory compression molding machine (Collin, P200E). Small pieces of blend materials were first sandwiched between aluminum sheets and then compressed following a specifically optimized temperature, pressure, and time program.
All samples were hot pressed at 180 °C to realize 0.2 mm thick sheets, from which the specimens were obtained. Table 1 reports composition of different formulations of PLASA. PLASAW samples were obtained from PLASA after immersion in water for 15 days and particles leaching.

Table 1. Composition, Glass Transition Temperature (T_g), Crystallization Temperature (T_c), Melting Temperature (T_m), and Degree of Crystallinity (X_c) for PLLA and PLASA as Evaluated on the Second Heating Scan

	Composition (%)						
Sample	**PLLA**	**SAP**	T_g (°C)	T_c (°C)	T_m (°C)	X_c (%)[b]	X_c (%)[c]
PLLA	100	—	60.0	—	—	4.8	0
PLASA10	88.8	11.2	59.6	130.5	153.8	0	1.8
PLASA20	77.3	22.7	59.6	130.0	153.6	0	1.8
PLASA30	68.7	31.3	59.4	128.7	153.5	0	2.2
PLASA50	50.2	49.8	59.2	125.2	150.4[a]	0	0
					156.64		
PLASA50W			59.0	121.0	150.84[a]	0	0
					157.25		

[a] Two melting peaks are found in some PLLA polymer derivatives and they were attributed to slow rates of crystallization and recrystallization[20]
[b] Crystallinity of the samples after processing has been calculated from the first heating scan.
[c] Crystallinity of the samples after processing has been calculated from the second heating scan.

Thermomechanical and Morphological Analysis

Tensile tests were performed by an electromechanic dynamometer (Instron Model 3366). Elastic modulus (E), strength (σ_b), and elongation at break (ε_b) were determined on 0.2 mm thick and 10 mm wide strips, with a gauge length of 80 mm tested at a crosshead speed 2 mm/min. Tensile tests were performed at room temperature after having conditioned the specimen at 55 °C for 4 h under vacuum to remove humidity potentially trapped in the composites.

Dynamic-mechanical thermal analysis was performed on specimens under tensile configuration by means of a DMA apparatus (DMA Q800 TA Instruments). Rectangular specimens (gauge length: 20 mm; width: 7 mm; thickness: 0.15–0.20 mm) were subjected to temperature sweep tests, carried out at 1 °C/min on a temperature interval between room temperature and 130 °C, at a frequency equal to 1 Hz and under displacement control (displacement amplitude: 15 μm).
Fracture tests were carried out on single edge notched in tension, SE(T), specimens obtained from the 0.2 mm thick sheets (nominal dimensions: width, $W = 14$ mm; initial crack length to width ratio, $a_0/W = 0.5$; distance between the grips, $h_0 = 30$ mm). SE(T) specimen used is represented in Figure 1. The sharp notch was introduced into the specimen by razor-blade sliding. Tests were carried out by using the Instron test system, with a crosshead speed of 1 mm/min, at room temperature. Stiff clamps were employed in order to avoid specimen rotation. Data were processed according to linear elastic fracture mechanics. Fracture initiation was assumed to occur at the peak of the load versus displacement curve recorded in the test, and the corresponding value of stress intensity factor (mode I of fracture), $K_{I,\text{peak}}$, was considered as the material fracture toughness, K_{Ic}, in plane-stress conditions. $K_{I,\text{peak}}$ was evaluated as [21]:

$$K_{I,\text{peak}} = \frac{P_{\text{peak}}}{B \cdot \sqrt{W}} \cdot f\left(\frac{a_0}{W}\right) \tag{1}$$

where P_{peak} is the peak-load, B is the specimen thickness, a_0 is the initial crack length (measured after the test on the fractured specimen by means of a travelling microscope), and $f(a/W)$ is the dimensionless geometry function [21]:

$$f\left(\frac{a}{W}\right) = \frac{\sqrt{2\tan\frac{\pi a}{2W}}}{\cos\frac{\pi a}{2W}}\left[0.752 + 2.02\left(\frac{a}{W}\right) + 0.37\left(1 - \sin\frac{\pi a}{2W}\right)^3\right] \tag{2}$$

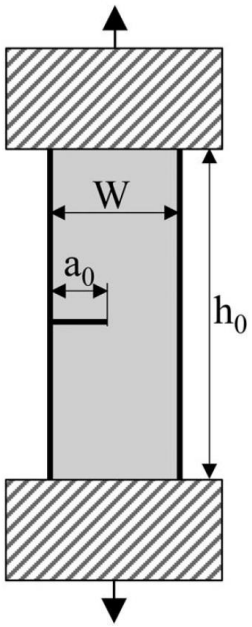

Figure 1 Schematic of the SE(T) specimen used in the fracture tests.

At least three different specimens each material examined (PLLA, PLLAW, PLASA30, PLASA30W).

Thermal analysis was performed in nitrogen atmosphere with a differential scanning calorimeter (DSC Q100, TA Instruments) at 10 °C/min heating rate. The glass transition temperature is taken as the inflection point of the change in heat capacity versus temperature on the second heating scan after cooling at 10 °C/min. The degree of crystallinity, X_c of the PLLA phase can be calculated based on the enthalpy value of a 100% crystalline PLLA as follows:

$$X_c = (\Delta H_m - \Delta H_c)100/\Delta H_m^\circ \quad (3)$$

where ΔH_m and ΔH_c designate the measured melting and crystallization enthalpy respectively, while ΔH_m° represents the reference enthalpy of melting for 100% crystalline PLLA which is 93.6 J/g [22]. The thermal decomposition of the materials was investigated by means of thermogravimetric analysis (TGA) using a TA Instrument (TGA Q500, TA Instruments). The weight loss and its first derivative were recorded at a dynamic heating rate of 50 °C/min as a function of temperature. Scanning electron microscopy (SEM) was used to examine the morphology of the systems using a LEO EVO 40 SEM. The compression molded specimens were cryogenically fractured in transverse direction. Samples were mounted with carbon tape on aluminum stubs and then sputter coated with gold to make them conductive prior to SEM observation.

Swelling Tests

Swelling capacity was evaluated by a modification of tea-bag method [23]. The tea bag (i.e., a filter paper Whatman grade 5) containing an accurately weighed sample was immersed in distilled water (200 mL), and allowed to soak for fixed intervals at room temperature. The tea bag was hung up for 5 min in order to remove the excess solution. The weight uptake after immersion in water was measured twice using the following equation:

$$\text{Swelling capacity} = \frac{W_2 - W_1}{W_1} 100 \quad (4)$$

where W_1 and W_2 denote the weight of dry and swollen specimen, respectively.
Weight loss was evaluated after SAP particles leaching by measuring the weight of dry specimen after immersion in water for fixed intervals as:

$$\text{Weight loss} = \frac{W_1 - W_3}{W_1} 100 \quad (5)$$

where W_1 and W_3 denote the weight of the starting dry specimen and that of the dry specimen after water immersion, respectively. In order to promote complete particles leaching and the achievement of a stable, well-structured microporous structure, the samples were immersed in water for 10 days and then dried at 50 °C under vacuum for 12 h.

Density and Porosity Evaluation

The porosity of samples after water immersion and particles leaching was measured using liquid substitution method [24]. Ethanol was used as the displacing liquid because it penetrates easily into the pores of the sample, but not into the PLLA itself. A sample of measured weight W was immersed in a graduated cylinder containing a known volume (V_1) of ethanol and kept for 5 min to allow the ethanol to penetrate into the pores of the sample. The total volume of the remaining ethanol and the ethanol-impregnated sample was then recorded as V_2 by simply reading the level in the cylinder. The volume difference ($V_2 - V_1$) represents the volume of the sample material. The ethanol-impregnated sample was then removed from the graduated cylinder and the residual ethanol volume was recorded as V_3. Hence the total volume of the sample was $V = (V_2 - V_3)$ and the bulk density of the material was expressed as:

$$\rho = W/(V_2 - V_3) \quad (6)$$

By measuring the initial and final weights W_i and W_f, respectively, of the sample after soaking in ethanol ($\rho_{ethanol} = 0.789$ g/cm^3) the pore volume of a sample can be calculated as $(W_f - W_i)/\rho_{ethanol}$ and the porosity can be measured using the following equation:

$$\text{Porosity} = \frac{\frac{W_f - W_i}{\rho_{ethanol}}}{V_2 - V_3} \quad 100 \qquad (7)$$

Shear ViscosityMeasurements

Complex dynamic viscosity of PLASA blends was measured with a plate-plate geometry by a Rheometrics RDA II rheometer at 180 °C in the 1–50 Hz frequency range. Specimens were maintained in desiccator before measurements.

RESULTS AND DISCUSSION

Various materials, coded PLASA (Table 1), were prepared by melt blending of different component amounts. After blending, the resulting material appeared visually homogeneous and the components well dispersed.

Figure 2 shows SEM micrograph of the PLASA30 composite. At the magnification level employed, a fairly homogeneous dispersion of particles was observed in the composite, showing a biphasic system with a regular distribution of particles, with diameter up to about 50 μm, within the PLLA polymeric matrix. Some particle sizes ranging from 5 to 10 μm are apparently impregnated inside the PLLA matrix [Figure 2 (b)], but in general it is evident a poor adhesion and low interaction between the particles and the matrix as suggested by the discontinuous aspect of the surface between the matrix and the particles. SAP particles are composed of a covalently crosslinked hydrophilic polyelectrolyte, that is, a polymer with ionizable groups such as sodium acrylates that can dissociate in solution. The high concentration of ions inside the SAP lead to a water flow into the SAP due to osmosis and, in addition, water solvation of hydrophilic groups present along the macromolecular network further increases the swelling capacity. Therefore, being the functional groups of SAP particles involved in the crosslinking reactions as well as in the sodium salt formation, during melt blending they are less available for both physical and chemical interactions with the PLLA matrix, as revealed by the results of this article. On the other hand, weak interactions with the matrix could promote the maintenance of the original SAP structure and superabsorbent properties.

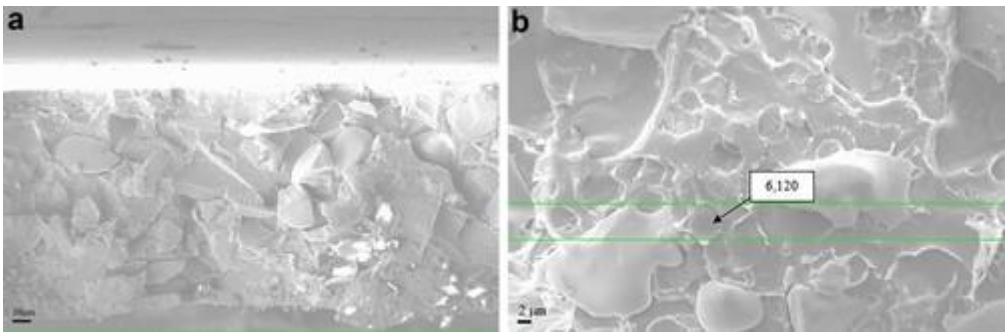

Figure 2 SEM micrographs of PLASA30 view from core to the surface, (a) scale bar of 10 μm ×1200 magnification, (b) scale bar of 2 μm ×4500 magnification.

This polymeric biphasic system shows excellent swelling properties, demonstrating that crosslinked particles retain their superabsorbent ability even if distributed in a thermoplastic polymeric matrix (Scheme 1).

Scheme 1 Mechanism of particles swelling and leaching out of the PLLA matrix.

The swelling or water uptake property of SAP materials is very important for applications. Figure 3 (a,b) summarizes, respectively, the swelling behavior and weight loss of the PLASA with different SAP content over time. The equilibrium swelling ratio and weight loss of PLLA (not shown in Figure 3) were negligible (i.e., <0.1%) while they increased with the SAP content in PLASA derivatives. The time to reach swelling equilibrium was about 3 h. As shown in Figure 3, the particles swell and simultaneously leach out of the matrix thus avoiding high volumetric expansion that could cause cracking or breaking of the stiff and brittle PLLA matrix. In particular, the equilibrium absorbency capacity of PLASA30 in water, evaluated by a modification of tea-bag method[23] was 3500% which indicates a water uptake about 35 times larger than its original weight. If compared with the free counterpart, the SAP particles on PLLA matrix maintain about 80% of the original absorbency capacity. The reduced absorbency capacity may be due to the probable presence of very small sodium polyacrylate particles size originated during compounding in the discontinuous mixer. These very small sodium polyacrylate particles apparently became impregnated inside the PLLA matrix rather than the other particles [Figure 2(a,b)], which would explain the decreased water absorbency of these powders[25]. In addition, according to Jensen and Hansen,[26] the small particles have decreased water absorbency because their surfaces are less active for water absorption than is the bulk of the SAP[27]. After water treatment, the particles swell and possibly due to the weak interaction with the matrix, are leached from PLLA generating increasing porosity with increasing starting SAP particles (Table 2). SEM micrographs of the sample PLASA50 after immersion in water for 15 days so to properly leach the SAP particles (i.e., PLASA50W, Figure 4) reveals a macroporous network material with pores, channels, and interstices of different sizes well interconnected and distributed into the material. Porous structure denotes a difference of porous morphology between the bulk and the surface where there is a thin skin with holes probably left by particles leaching during water treatment. In addition, the high magnification micrograph [Figure 4 (b)] reveals interconnected cavities with a relatively smooth surface.

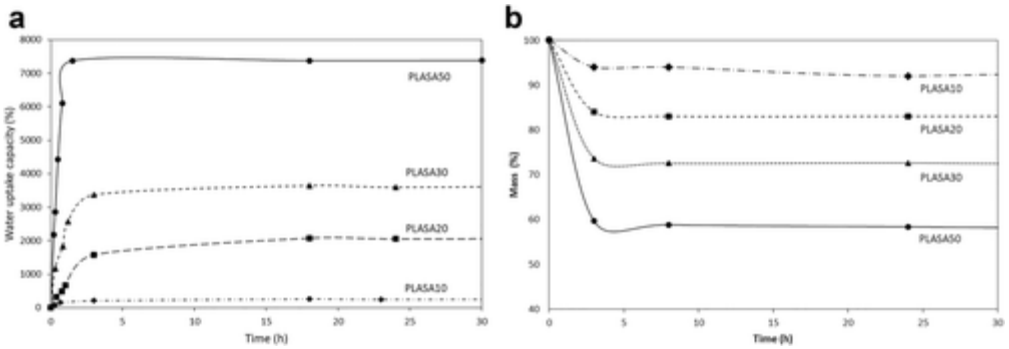

Figure 3 (a) The swelling behavior and (b) mass retention of the PLASA derivatives having different SAP content.

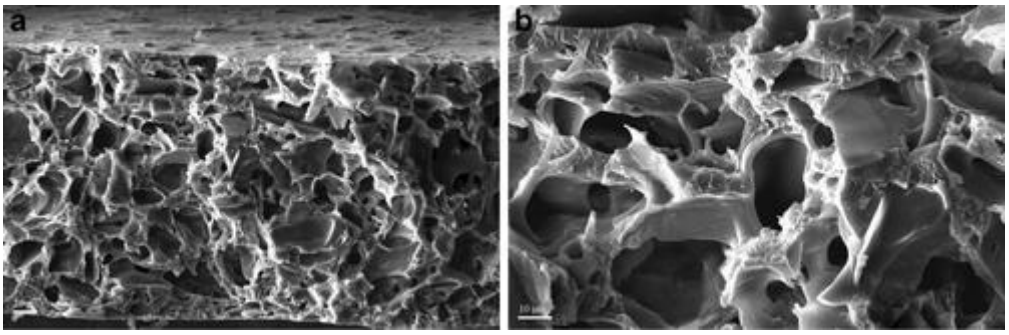

Figure 4 SEM micrographs of PLASA50W (i.e., after water treatment for 15 days) view from core to surface: (a) scale bar of 20 μm ×800 magnification, (b) scale bar of 10 μm ×2500 magnification.

Density and porosity of pure PLLA and of PLASAW samples obtained after swelling of PLASA in water (Table 2) were measured using liquid substitution method. As expected, reduced density and increased porosity were observed on the samples as results of the increased amount of leached particles. It is important to mention that PLASAW samples maintain shape integrity, and no significant deformations were observed during water treatment. In addition, the samples seem to maintain good mechanical properties even at high porosity since they are easily manipulated and processed.

Table 2. Density and Porosity of PLLA and PLASAW Evaluated by Liquid Substitution Method[24]

Sample	Density (g/cm^3)	Porosity (%)
PLLA	1.29	0.6
PLASA10W	0.73	28.7
PLASA20W	0.64	30.1
PLASA30W	0.46	59.9
PLASA50W	0.26	79.5

To elucidate the role of the filler (i.e., polymeric crosslinked SAP particles) on the overall physical-mechanical behavior of PLLA matrix, tensile tests, DMA, and fracture tests were performed on the various materials. It was found that the mechanical properties are markedly modified by addition of crosslinked particles which induce a regular stiffening effect. The overall dependence of tensile properties on initial filler amount is summarized in Figure 5. In particular, Figure 5 (a) represents the Young's modulus as a function of the initial SAP content of all composite materials, before and after water immersion. In PLASA materials the Young's modulus increases regularly with the SAP content. Removal of SAP particles leads to the obtainment of porous materials whose porosity increases with the starting amount of SAP. This explains the reduction of Young's modulus observed in PLASAW as a function of the SAP content. Both the presence of filler and voids, which act as defects, determines a reduction of material strength [Figure 5 (b)]. In particular, if compared with pure PLLA a strength reduction of about 14% and 70% is observed as a consequence of SAP particles introduction and removing, respectively, from PLASA10. A further increase of the starting SAP content induces only a slight reduction of strength in the porous systems. The abatement of material resistance in porous PLLA is probably due to some microcracking occurring during the initial steps of swelling as a consequence of a slight volume expansion of the matrix. Then the particles can leach out from the matrix without any significant expansion. Both in PLASA and in PLASAW the elongation at break is only slightly affected by the initial amount of SAP, which does not alter significantly the inherently brittle behavior of PLLA [Figure 5 (c)].

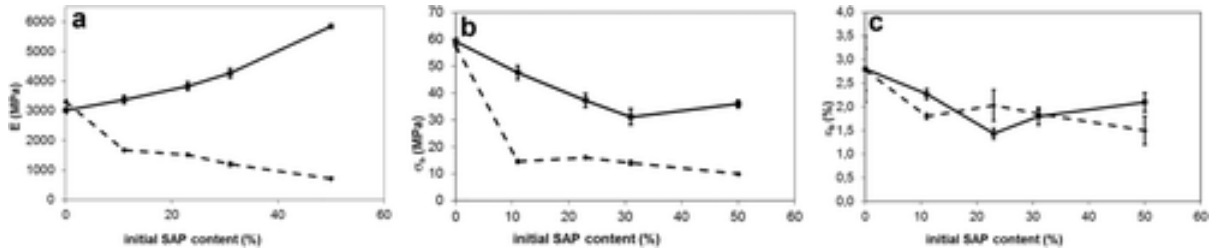

Figure 5 Young's modulus (E) (a), tensile strength (σ) (b), and elongation at break (ε_b) (c) of different PLASA (continuous line) and PLASAW (dashed line) as function of starting SAP content.

The results of the dynamic-mechanical analysis are reported as storage modulus, E', and loss modulus, E'', versus temperature traces in Figure 6 (a,b), respectively. The curves refer to the first heating scan applied in dynamical-mechanical tests to neat PLLA and various PLASA systems (PLASA30; PLASA50; PLASA30W), so to characterize their response in the as-produced state.

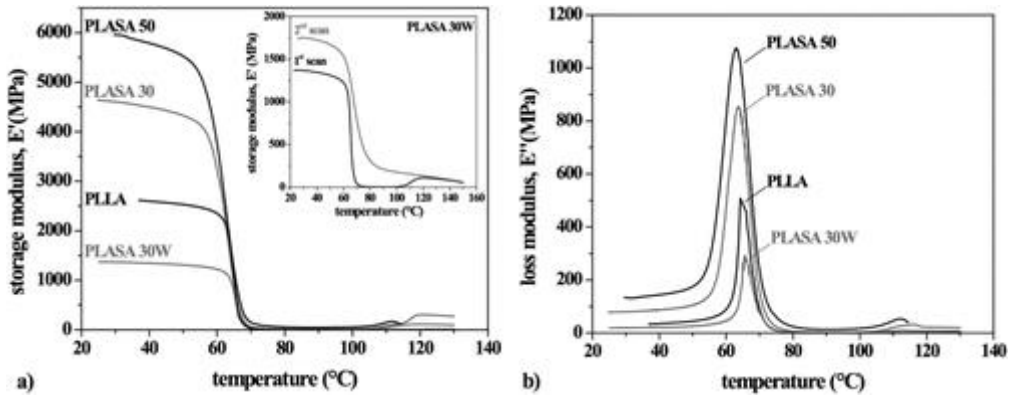

Figure 6 (a) Storage modulus and (b) loss modulus as a function of temperature for neat PLLA, PLASA system with different SAP contents (PLASA30, 30 wt %; PLASA50, 50 wt %), and system PLASA30 after immersion and particles leaching (PLASA30W). Inset of (a), storage modulus traces for the system PLASA30W after two subsequent heating scans.

All the materials present a similar dependence of the storage modulus on temperature, and mainly differ for the E' values at low temperatures. All the materials behave as relevantly stiff (the storage modulus ranging between 1 and 6 GPa at room temperature) up to at least 55 °C; subsequently, an abrupt modulus drop is found on a narrow region at slightly higher temperatures (about 60 °C), and a final increase for temperatures above 90 °C, finally leading to storage modulus values between 100 and 200 MPa.

The sharp storage modulus drop and subsequent increase suggests that the material, in its as-produced state, incorporates a relevant fraction of amorphous phase, and undergoes a recrystallization process only at temperatures well above T_g. To verify the occurrence of the recrystallization process the various systems were subjected to two subsequent heating scans, whose comparison is reported in the case of system PLASA30W in the inset of Figure 6 (a), and being similar for all the specimens investigated. The second heating scan on the specimen clearly shows that the development of a crystalline phase promotes an increase of the low temperature modulus of about 20% with respect to the values measured in the first heating scan, and an increase of the glass transition temperature of about 5 °C; as expected, the first and second heating scan traces tend to converge to a same behavior above the recrystallization region.

By comparing the E' and E'' traces of the various systems, it is possible to see that incorporation of the filler promotes a significant increase of the room temperature stiffness, while the trace of a PLASA30 system after prolonged immersion (i.e., system PLASA30W) shows that when the particles leach out lower room temperature, modulus values are found as a consequence of the highly porous structure. The presence of the SAP particles partially limits the entity of the modulus drop at T_g, and while neat PLLA approaches minimum modulus values around 1 MPa, that of

PLASA50 attains values of about 100 MPa. Nonetheless, for all the materials the recrystallization process occurs, as shown by the modulus rise well above T_g. On the other hand, a broader transition region is found on the higher particles content [see Figure 6 (b)], accompanied by a slight reduction of the glass transition temperature (evaluated as E'' peak), probably as a consequence of a larger chain mobility at the polymer-particle interface, due to the low adhesion.
The loading curves recorded in the fracture tests carried out on neat PLLA, water immersed PLLA (PLLAW), PLASA30, and PLASA30W show an increase in load followed by an abrupt drop at load-peak. Nonlinear effects, observed mainly for PLASA30W sample, were neglected for fracture toughness determination. Plane-stress fracture toughness data ($K_{I,\text{peak}}$) evaluated for the various samples are reported in Table 3 (specimen thickness of 0.2 mm). By comparing fracture toughness of PLASA30 with that of neat PLLA, it emerges that the incorporation of SAP particles into PLLA promotes a 61% decrease in toughness. Interestingly, a similar reduction of fracture toughness (66%) is observed by comparing PLASA30W with PLLAW. This suggests, at a macroscopic scale, that porosity formation after prolonged immersion in water for PLASA30 does not promote an embrittlement effect more pronounced than that induced by SAP particles incorporation in PLLA, despite of its intrinsically highly defective structure.

Table 3. Fracture Properties of PLLA and PLASA Derivatives

Sample	$K_{I,\text{peak}}$ (MPa m$^{0.5}$)
PLLA	8.9 ± 1.36
PLLAW	5.3 ± 0.49
PLASA30	3.5 ± 0.24
PLASA30W	1.8 ± 0.11

Since crystallinity is seen as not fully developed in the various PLASA systems, and since the crystallinity content may strongly influence the mechanical properties, the thermal properties of SAP derivatives were studied through DSC test. DSC analysis of SAP did not evidence transitions. Table 1 listed glass transition temperature (T_g), crystallization peak temperature (T_c), and melting peak temperature (T_m) for PLLA, different PLASA, and PLASAW, as evaluated on the second heating scan. T_g remained almost unchanged since only small differences, within 1 °C, were recorded. Usually the T_g of a polymeric matrix tends to increase with the addition of particles or nanoparticles, due to interactions between the polymer chains and the particles and also due to the reduction of the macromolecular chain mobility in the zone surrounding the particles. However, in this study, it seems that the chain segment mobility of the PLLA phase was not influenced by the introduction of SAP particles suggesting a reduced filler-matrix interaction. The initially crystalline PLLA presented a T_g at 65.2 °C and T_m at 154 °C. During cooling, no crystallization was recorded and the following second heating run on the amorphous materials showed T_g at 60.2 °C (Figure 7). On the other hand, for all PLASA derivatives the crystallization and cold crystallization temperatures decrease with increasing amount of SAP particles, as a consequence of nucleation effect promoted by SAP particles on PLLA crystallization. A similar effect was observed on the sample after expulsion of SAP particles where the cold crystallization temperature decreases to 121 °C.

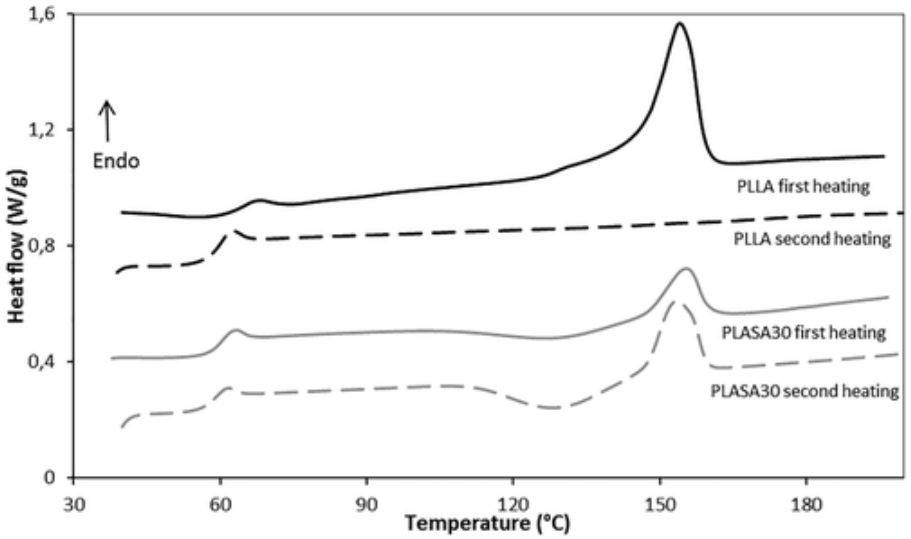

Figure 7 DSC thermal cycles of PLLA (black) and PLASA30 (gray) (first and second heating at 10 °C).

SAP particles can also influence the thermal stability of the polymer, this is very important during polymer processing, for example, in the case of melt extrusion or injection molding. Therefore, thermal degradation of the PLASA derivatives were studied by TGA. TGA and the derivative thermogravimetric curves of PLLA and PLASA are shown in Figure 8 (a,b).

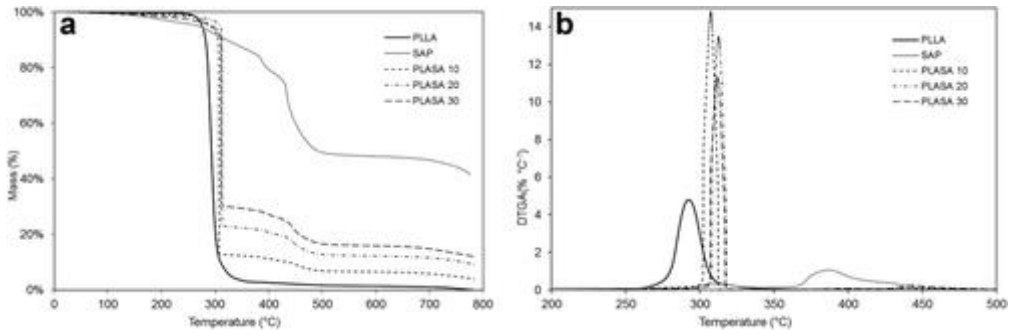

Figure 8 Thermogravimetric (TGA) (a) and derivative thermogravimetric (DTGA) (b) curves of PLLA, PLASA10, PLASA20, and PLASA30.

Thermal degradation of PLLA appears to be relevant only at temperatures above 260 °C and its maximum decomposition rate is at 293 °C. PLASA derivatives show a negligible loss of about 1% at temperature ranging from 100 to 150 °C probably due to the absorbed water and the decomposition begins at higher temperature (about 260–270 °C). Their maximum decomposition rate is above 307 °C and increases up to 313 °C with SAP content indicating an improvement in thermal stability of PLASA derivatives as compared to that of neat PLLA. Furthermore, due to the presence of inorganic moiety on SAP (crosslinked sodium polyacrylate), PLASA derivatives do not complete the decomposition up to 800 °C but a persistent residue, increasing with SAP amount, remains.

In order to estimate processability of the materials, complex viscosity (η*) of PLASA at 180 °C was measured as function of frequency. The results indicate that the presence of SAP particles in PLASA systems induce a decrease in viscosity, with respect to neat PLLA (Figure 9). As already pointed out, PLLA is quite sensitive to degradation induced by presence of even small amount of absorbed water. The presence of SAP makes the material desiccation before processing even more necessary; yet complete removal of water is extremely difficult also considering that water regain is very fast (Figure 3). TGA results [Figure 8 (a)] confirm that SAP particles increase the weight loss at low temperatures due to absorbed water compared to pure PLLA, notwithstanding this moisture content is remarkably small (<1% as indicated above). The presence of such small amount of

absorbed water may induce molecular weight reduction during processing, as well as during the rheological tests, and this would lead to a viscosity decrease.

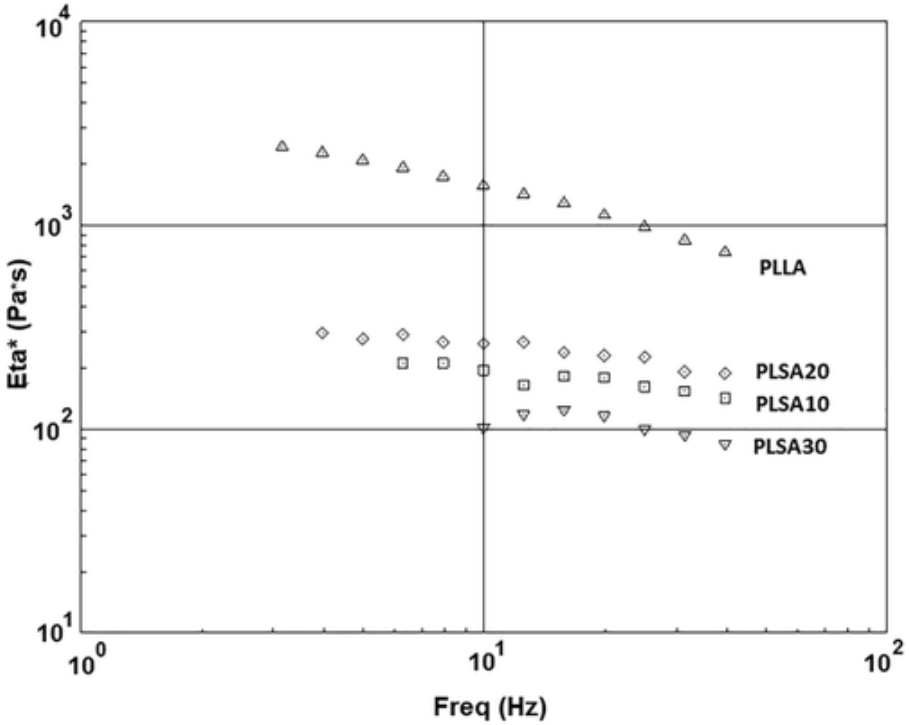

Figure 9 Complex viscosity curves at 180 °C of PLLA and PLASA with different SAP content.

CONCLUSIONS

Superabsorbent PLLA-based thermoplastic composite materials with good mechanical properties have been prepared from melt-processed PLLA/SAP particles binary system. The polymeric biphasic system, showed excellent swelling properties, demonstrating that crosslinked particles retain their superabsorbent ability even if distributed in a thermoplastic polymeric matrix. The thermal characteristics of the biocomposites evidence enhanced thermal stability in comparison with neat PLLA and also mechanical properties are markedly modified by addition of crosslinked particles which induce regular stiffening effect. Furthermore, in aqueous environments the particles swell and are leached from PLLA matrix generating a macroporous network with interconnected porosity of about 80% void volume.
Although PLASA derivatives showed good mechanical properties and excellent water uptake capacity, being water uptake irreversible after particles leaching, it is not clear whether or not these derivatives are suitable for SAP materials. On the other hand, the new open pore PLLA-based foams, produced after particles leaching in the absence of organic solvents and chemical foaming agents, appear very promising for scaffold production. In fact, open porosity is a crucial point because scaffold must possess a highly porous structure with a fully interconnected geometry to provide cell ingrowth and survival and uniform cell distribution.

ACKNOWLEDGMENT

The contribution of Gloria Spagnoli and Isabella Peroni in the experimental testing is gratefully acknowledged.

REFERENCES

1. Buchholz, F. L.; Graham, A. T. Modern Superabsorbent Polymer Technology; Wiley-VCH: New York, 1998; Chapter 1–7.
2. Horie, K.; Baròn, M.; Fox, R.; He, J.; Hess, M.; Kahovec, J.; Kitayama, T.; Kubisa, P.; Marechal, E.; Mormann, W. Pure Appl. Chem. 2004, 76, 889.
3. Liu, C. H.; Chen, Y. Q.; Chen, J. G. Carbohydr. Polym. 2010, 79, 500.
4. Viseras, C.; Cerezo, P.; Sanchez, R.; Salcedo, I.; Aguzzi, C. Appl. Clay Sci. 2010, 48, 291
5. Lee, W. F.; Yang, L. G. J. Appl. Polym. Sci. 2004, 92, 3422.
6. Kim, J.; Lee, K. W.; Hefferan, T. E.; Currier, B. L.; Yaszemski, M. J.; Lu, L. Biomacromolecules 2008, 9, 149.
7. Adhikari, B.; Majumdar, S. Prog. Polym. Sci. 2004, 29, 699.
8. Cannazza, G.; Cataldo, A.; De Benedetto, E.; Demitri, C.; Madaghiele, M.; Sannino, A. Water 2014, 2056.
9. Pourjavadi, A.; Ghasemzadeh, H.; Soleyman, R. J. Appl. Polym. Sci. 2007, 105, 2631.
10. Li, A.; Zhang, J. P.; Wang, A. Q. Polym. Adv. Technol. 2005, 16, 675.
11. Bessee, G. B. Keeping Jet Fuel Clean and Dry; Southwest Research Institute (SwRI): San Antonio, TX, 2017,
12. Aalaie, J.; Vasheghani-Farahani, E.; Rahmatpour, A.; Semsarzaden, M. A. Eur. Polym. J. 2008, 44, 2024.
13. Haraguchi, K.; Li, H. J. Macromolecules 2006, 39, 1898.
14. Zhu, M.; Xiong, L.; Wang, T.; Liu, X.; Wang, C.; Tong, Z. React. Funct. Polym. 2010, 70, 267.
15. Garlotta, D. J. Polym. Environ. 2002, 9, 63.
16. Auras, R.; Harte, B.; Selke, S. Macromol. Biosci. 2004, 4, 835.
17. Zang, J. F.; Sun, X. In Biodegradable Polymers for Industrial Applications; R. Smith, Ed.; CRC Press: Cambridge, UK, 2005; Chapter 10, p 251
18. Satyanarayana, D.; Chatterji, P. R. J. Macromol. Sci. RMC 1993, C33, 39
19. Cheung, H. Y.; Lau, K. T.; Lu, T. P.; Hui, D. Compos. B 2007, 38, 291.
20. Yasuniwa, M.; Tsubakihara, S.; Sugimoto, Y.; Nakafuku, C. J. Polym. Sci. Part B: Polym. Phys. 2004, 42, 25.
21. Anderson, T. L. In Fracture Mechanics: Fundamentals and Applications; CRC Press: Cambridge, UK, 2005.
22. Fisher, E. W.; Sterzel, H. J.; Wegner, G. Kolloid Z. Z. Polym. 1973, 251, 980.
23. Zohuriaan-Mehr, M. J.; Motazedi, Z.; Kabiri, K.; Ershad-Langroudi, A.; Allahdadi, I. J. Appl. Polym. Sci. 2006, 102, 5685.
24. Kothapalli, C.; Shaw, M.; Wei, M. Acta Biomater. 2005, 1, 653
25. Lee, J. H.; Lee, S. G. J. Appl. Polym. Sci. 2016, 133, DOI: 10.1002/app.43973.
26. Jensen, O. M.; Hansen, P. F. Cem. Concr. Res. 2001, 31, 647.
27. Rosa, F.; Bordado, J.; Casquilho, M. J. Appl. Polym. Sci. 2008, 107, 3413.